Appendix 1 Supplemental methods

Our developed framework is based on open-source software, Paraview v.5.9.0 (46) for pre-processing and visualization, complimented by in-house Python modules based on Simple ITK v.2.0.2 (47,48) for segmentation and quantification of the regions of interest (*Figure S1*; *Table S2*).

Image pre-processing

Initially, the volumetric CT images, with acquisition parameters detailed in *Table S1*, were loaded into Paraview and the opacity transfer function in the volumetric view was adjusted to highlight soft tissue in the thoracic CT scan, such as vessels and organs (*Figure 1A*). With the aorta clearly visible, the image was then cropped to have a field of view focused on the aortic root, including the interface between the aortic valve and the left ventricular outflow tract (LVOT), a part of the ascending aorta after the sino-tubular junction (STJ) and excluding any other surrounding structures (*Figure 1A*). The field of view is then resampled to have isotropic voxel dimensions of [0.5, 0.5, 0.5 mm].

Valve segmentation

To segment the valve from surrounding tissue, the fast-marching method was employed. This method is closely related to level-set segmentation which is based on solving a partial differential equation (PDE) named the *Eikonal* equation Eq. [1] (49)

$$|\nabla u| = C \tag{1}$$

Where u describes the evolution of a closed surface as a function of time and C represents the cost image which is modeled as the speed of the propagating surface. Fast marching has been shown to segment anatomical regions of complex topology and varied curvature (49). The segmentation process is controlled by seed points where it propagates outward from the local surface normal of the seed points (49). The propagation is controlled by the design of what is known as the speed image or function, which aims to incorporate image features such that high values are present near boundaries and lower values in homogenous regions (49). For our purposes, we first derived a smoothed gradient magnitude image using a gradient magnitude recursive gaussian operation (50) with a smoothing sigma of 0.5. The final speed image was then calculated using a bounded reciprocal operation (50) which produces a new image with values of zero near the boundaries or edges, and values of one in homogeneous regions. The determination of the cost function can be defined as in Eq. [2]

$$C(x) = \frac{1}{1 + |\nabla I_g(x)|} \tag{2}$$

Where $C(x)$ denotes the cost and $I_g(x)$ represents the image gradient at some index x. The centroid of the previously annotated field of view (*Figure 2A*) was used as initial seed point, along with the constructed speed image as inputs into a fast-marching procedure (50). The output of which is a time-crossing map, which indicates the time of arrival of the propagated level-set front. This arrival time effectively becomes the number of iterations required segment a particular structure. We therefore set a threshold for this output to a fixed time/level using a binary threshold (50) of 400 iterations, which, we deemed an appropriate value for segmenting the aortic root shape without the calcification in the leaflets. An important implication of how the cost function was designed, is that the segmentation propagates through luminal non-calcified segments that are smoother in the speed image and stop at calcified "sharp" edges in the gradient function.

Finally, to correct for noise and holes in the segmentation and obtain a smoothed surface, we initially used a morphological closing operation (50) with a kernel radius of 2 voxels, and then a smoothing recursive gaussian operation (50) with a kernel radius of 2 voxels. For visualizing the binary volume as a transparent surface, we used the contour filter (51) in Paraview on the final filter output shown in *Figure 1B*. The details of the processing pipeline are shown in a flowchart in *Figure S1* and the detailed parameterization for the various filters is presented in *Table S2*.
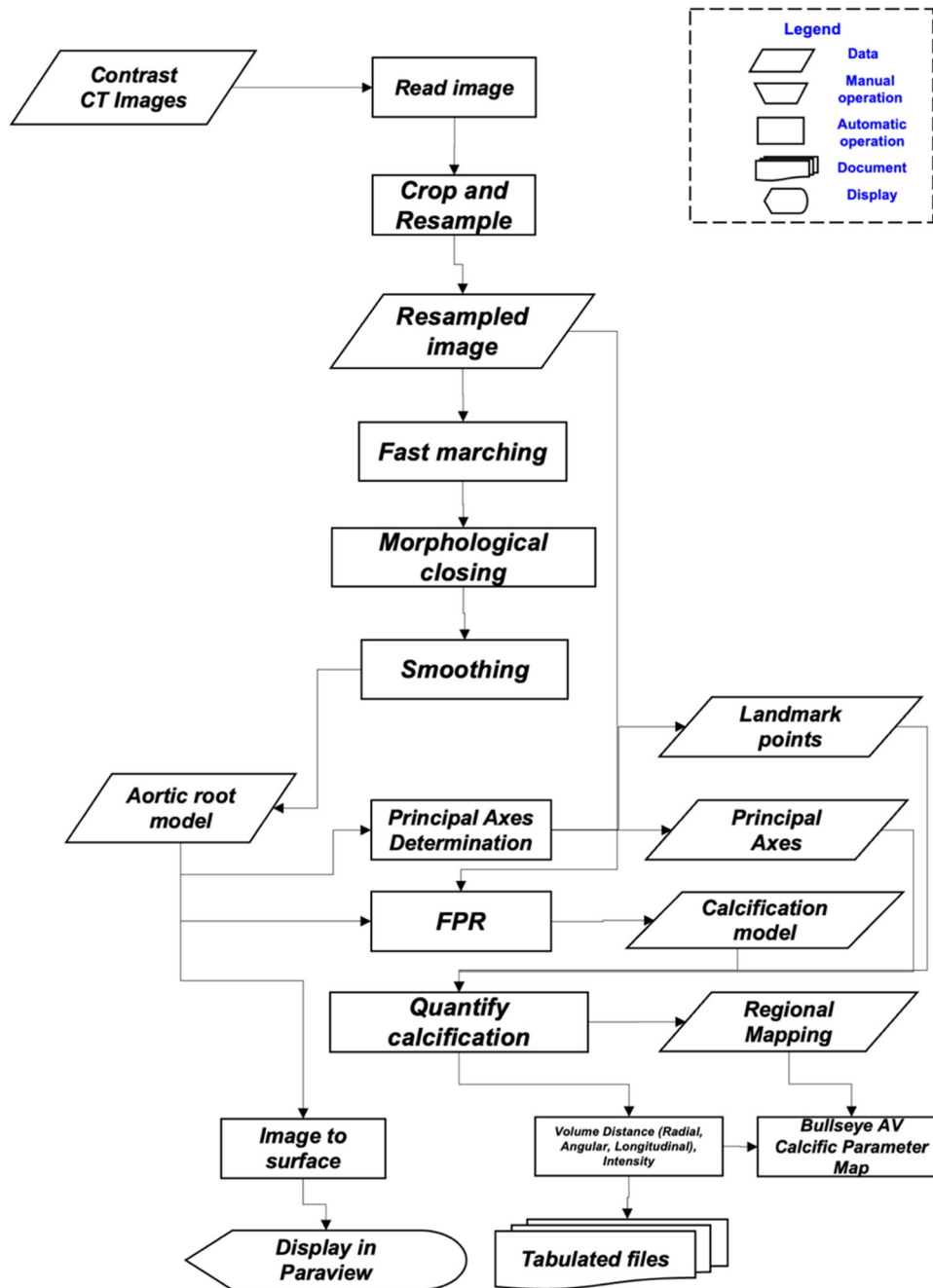
Figure S1 Flowchart diagram of the computational framework developed for assessment of calcification. The flowchart describes a series of operations, either manual or automatic that operate on an initial input set of CT images, to eventually generate tabulated files with relevant clinical indices such as volume scores and display 3D models of detected valve and calcification.

Principal axes determination and landmark points

Once, the smoothed aortic root model is constructed, we proceed to analyze the shape features of the binary segmentation. This is done through shape statistics algorithm (52), which allows us to automatically estimate the orientation axes, the center

Table S1 CT acquisition information

CT protocol information	CT scanning parameters
Acquisition	Retrospective gated
Slice thickness	0.625 or 3 mm
Tube rotation	0.35 s
Pitch	0.24:1
Tube voltage	120 kV
Tube current	400–500 mA
Reconstruction	ASIR at 30%
Cardiac phase selected	Best diastole (70–75%) cardiac cycle

CT, computed tomography; ASIR, adaptive statistical iterative reconstruction.

of mass and the boundary points of a binary object based on its topology (*Figure 1A*, *Figure S1*, *Table S2*). These principal axes correspond to anatomical short axis view, and two long axis views that are perpendicular to the "En-face" short axis view. These three orientation vectors can be manually corrected by the user, if necessary, to properly orient the desired anatomical views.

We require annotation of four landmark points to complete the analysis. The first landmark point is initialized from the center of mass of the aortic root model and is then corrected such that it falls at the level of the STJ plane and centered at the aortic annulus in the short-axis orientation *Figure 1C*. Next, using the estimated position of the center of the aortic root, the boundary points and the short-axis direction. We proceed to find the maximum elevation points in a directed direction towards the LVOT. These points are then filtered to localize probable location of valve hinge points. The initial location of these three points is corrected manually, such that the points are centered at each cusp and ordered sequentially as NCC, RCC, LCC, respectively *Figure 1D*.

The final STJ point and the orientation axes together uniquely define a new local coordinate system that is relative to the aortic valve leaflets. The basis vectors of this coordinate system *A* can be computed as an affine transformation Eq. [3], consisting of a rotational Eq. [4] and a translational component Eq. [5]

$$A = \begin{bmatrix} R & b \\ 0\cdots 0 & 1 \end{bmatrix} \tag{3}$$

such that

$$R = R_z(\gamma) R_y(\beta) R_x(\alpha) = \begin{bmatrix} \cos\gamma & -\sin\gamma & 0 \\ \sin\gamma & \cos\gamma & 0 \\ 0 & 0 & 1 \end{bmatrix} \begin{bmatrix} \cos\beta & 0 & \sin\beta \\ 0 & 1 & 0 \\ -\sin\beta & 0 & \cos\beta \end{bmatrix} \begin{bmatrix} 1 & 0 & 0 \\ 0 & \cos\alpha & -\sin\alpha \\ 0 & \sin\alpha & \cos\alpha \end{bmatrix} \tag{4}$$

and $b = \begin{bmatrix} C_x \\ C_y \\ C_z \end{bmatrix}$ [5]

The original frame of reference is represented as x, y, z corresponding to anatomic sagittal, coronal, and axial views, respectively (*Figure 1A*, left panel). The rotation angles required to transform the original frame of reference to the local frame are determined from the final "En-face" short axis plane normal (*Figure 1A*, right panel), yielding rotations about the original frame with angles α, β, γ respectively about each axis Eq. [3]. The translation vector b is determined from STJ landmark point defined as C_x, C_y, C_z. The entire affine transformation is later used to realign the image direction, so that the long axis of the valve is now parallel to the unit z and leaflet faces are parallel to the $z = 0$ plane. This is necessary to accurately determine the spatial position of calcific voxels for distance map generation.

Table S2 Overview of operations/filters used in the platform, input, output and parameters used where applicable

Procedure	Input	Value	Output
Crop and resample	Size	Patient specific	Resampled image [image (HU)]
	Resolution	0.5 mm	
Fast marching	Speed sigma	0.65	Binary mask
	No. of iterations	300	
	Seed point location	Center of aortic root [1]	
Morphological closing	Kernel radius	2	Binary mask
Smoothing	Sigma	0.5	Aortic root model (binary mask)
	Kernel radius	2	
Principal axes determination	Aortic root model	Binary mask [4]	Direction matrix
			Shape boundary
			Geometric center
FPR	Aortic root model	Binary mask [4]	Calcification model (binary mask)
	Resampled image	Image (HU) [1]	
	False positive rate threshold	0.01 = 1%	
Quantify calcification	Calcification model	Binary mask [6]	Regional calcification map (binary mask)
	Principal axes orientation	3×3 direction matrix [5]	Radial distance map (image [mm])
	Landmark points	4 points [5]	Longitudinal distance map (image [mm])
	Volume	Binary mask [6]	Calcification intensity map (image [HU])
Regional mapping	STJ height	Patient specific	Anatomical 18 region volume map
	Annular radius	Derived from patient specific annular area	
	Interleaflet triangle angles	Patient specific	Anatomical 18 region average intensity map
	Calcification model	Binary mask [6]	
	Principal axes orientation	3×3 direction matrix [5]	

Calcium detection [false positive rate (FPR) method]

When viewing the aortic valve (AV) region of interest (ROI) in cases of AS from CT images, we can observe disconnected groups of calcific lesions. These lesions are presented as relatively brighter intensities compared to tissue and lumen. The presence of the contrast agent makes the lower and upper bounds of these intensities practically unknown which is in part due to differences in contrast absorption for each patient (53). Therefore, given that the calcific intensity average will be statistically higher than surrounding objects, a procedure that can grow iteratively from an initial HU estimate is required. The initial estimate of calcific HU threshold is based on average HU of the partial aortic root model. In our proposed implementation we proceed based on the following steps. Using the initial HU estimation, we iteratively increase the HU threshold in steps of 1 HU unit. This is performed exhaustively until a minimum false positive rate criteria is reached (1%).

$$FPR = \frac{C / AR}{C} \qquad [6]$$

The (FPR) is defined (54) in set notation as: the ratio between, the no. of pixels in the set difference (/) of the aortic root model (AR) segmentation from the calcification model (C) and the total no. of pixels in the calcification model. As the

threshold is increased, we expect this rate to decrease as the number of luminal pixels mislabeled as calcific decreases. This representation yields a non-linear relationship between the rate and HU threshold of detection which can then be treated as a constrained global minimization problem *Figure 2C*. However, the discrete function representation does not have a global minimum and a specific constraint must be set to avoid overshooting an optimal threshold. We used a minimum of 0.01/1% FPR to stop the iterations and find the optimal threshold. We expect that iterative scheme combined with a global constraint can yield calcific detection thresholds that are robust to variations in intraluminal contrast, calcific density and other image specific factors.

The flowchart of the calcification detection pipeline is shown in *Figure S1* and the parameters used to initialize the shape overlap algorithm is presented in *Table S2*.

Volume and geometric analysis

The final segmented calcium region (*Figure 2A,2B*, red region) is presented as a binary image with values of one in pixels where calcium was detected and values of zero in pixels lacking calcium. We can proceed to determine the volume score based on Eq. [7]

$$Vs = \left(\sum_{i=0}^{N} M_i \right) \times 0.5^3 \qquad [7]$$

A volume score Vs is calculated by multiplying the total count of ones present on the binary image matrix with the image spacing. Where M_i represents the value of the pixel at index i and N is the total number of pixels. The image spacing due to the previous uniform resampling is 0.5 as mm per direction, giving a total volume score in mm^3.

Since the image volume is now oriented with the long axis of the valve parallel to the Z unit vector, topographic distance maps of the segmented calcium volume can be generated by first converting all pixel coordinates into a physical cartesian coordinate space using the conversion in Eq. [8]

$$\begin{pmatrix} P_1 \\ P_2 \\ P_3 \end{pmatrix} = \begin{pmatrix} O_1 \\ O_2 \\ O_3 \end{pmatrix} + \begin{pmatrix} 1 & 0 & 0 \\ 0 & 1 & 0 \\ 0 & 0 & 1 \end{pmatrix} \times \begin{pmatrix} 0.5 & 0 & 0 \\ 0 & 0.5 & 0 \\ 0 & 0 & 0.5 \end{pmatrix} \times \begin{pmatrix} I_1 \\ I_2 \\ I_3 \end{pmatrix} \qquad [8]$$

$$\begin{pmatrix} P_1' \\ P_2' \\ P_3' \\ 1 \end{pmatrix} = A. \begin{pmatrix} P_1 \\ P_2 \\ P_3 \\ 1 \end{pmatrix} \qquad [9]$$

Where $\vec{P}$ represents the resulting physical space position of an image pixel at some index $\vec{I}$, and $\vec{O}$ is the physical space origin of the first image index. This transformation is automatically handled using the function transform index to physical point (50) and repeated for each pixel index in the image volume. Next, we need to change the basis of each physical coordinate to the local aortic valve system we previously defined in section Calcium detection (shape overlap method). This is accomplished by simple dot product with the transformation matrix that defines the new system Eq. [9].

A conversion from cartesian to cylindrical coordinates can then be applied to $\vec{P}$ for each image pixel, using the transformation in Eq. [10].

$$r = \sqrt{P_1'^2 + P_2'^2}; \quad \theta = \tan^{-1}\left(\frac{P_2'}{P_1'} \right); \quad l = P_3' \qquad [10]$$

These transformations enable the generation of both radial and longitudinal distance maps relative to the aortic sinuses landmark point (*Figure 1B*). Image pixel values are set as r, θ or l for radial, angular and longitudinal maps respectively. These new distance image maps can be then used to introduce the anatomical regional mapping scheme in order to precisely quantify calcific content via the schematic described in *Figure 1C*. The regional map relies on successive binary thresholding

operations followed by a Boolean intersection (&) operation where in this case the thresholds are determined from the patient specific dimensions of the STJ Height (h), Annular area derived radius (r) and the specific interleaflet triangle angles that demarcate the angular extent of each leaflet (θ_{ncc}, θ_{rcc}, θ_{lcc}). The specific thresholds used as per the proposed 18 region map scheme *Figure 1C* is explicitly described in Eq. [11]. The specific percentage multipliers and patient specific ranges were based on common presentation of a normal tricuspid valve anatomy *Figure 1C* (37) and aim to equalize the area of each region to facilitate comparison with increasing angle divisions as we move towards the attachment from the coaptation zone and fixed radial intervals 0.5r apart.

$$R_n = \begin{cases} R_1\left(\sum R_i \& \sum A_i \& \sum L_i\right) & s.t.: 0 \le R_i < 0.25r;\ 0 \le A_i < \theta_{ncc};\ 0.5h \le L_i < h \\ R_2\left(\sum R_i \& \sum A_i \& \sum L_i\right) & s.t.: 0 \le R_i < 0.25r;\ \theta_{ncc} \le A_i < \theta_{rcc} + \theta_{ncc};\ 0.5h \le L_i < h \\ R_3\left(\sum R_i \& \sum A_i \& \sum L_i\right) & s.t.: 0 \le R_i < 0.25r;\ \theta_{rcc} + \theta_{ncc} \le A_i < \theta_{rcc} + \theta_{ncc} + \theta_{lcc};\ 0.5h \le L_i < h \\ R_4\left(\sum R_i \& \sum A_i \& \sum L_i\right) & s.t.: 0.25r \le R_i < 0.75r;\ 0 \le A_i < 0.5\theta_{ncc};\ 0.5h \le L_i < h \\ R_5\left(\sum R_i \& \sum A_i \& \sum L_i\right) & s.t.: 0.25r \le R_i < 0.75r;\ 0.5\theta_{ncc} \le A_i < \theta_{ncc};\ 0.5h \le L_i < h \\ R_6\left(\sum R_i \& \sum A_i \& \sum L_i\right) & s.t.: 0.25r \le R_i < 0.75r;\ \theta_{ncc} \le A_i < 0.5\theta_{rcc} + \theta_{ncc};\ 0.5h \le L_i < h \\ R_7\left(\sum R_i \& \sum A_i \& \sum L_i\right) & s.t.: 0.25r \le R_i < 0.75r;\ 0.5\theta_{rcc} + \theta_{ncc} \le A_i < \theta_{rcc} + \theta_{ncc};\ 0.5h \le L_i < h \\ R_8\left(\sum R_i \& \sum A_i \& \sum L_i\right) & s.t.: 0.25r \le R_i < 0.75r;\ \theta_{rcc} + \theta_{ncc} \le A_i < \theta_{rcc} + \theta_{ncc} + 0.5\theta_{lcc};\ 0.5h \le L_i < h \\ R_9\left(\sum R_i \& \sum A_i \& \sum L_i\right) & s.t.: 0.25r \le R_i < 0.75r;\ \theta_{rcc} + \theta_{ncc} + 0.5\theta_{lcc} \le A_i < \theta_{rcc} + \theta_{ncc} + \theta_{lcc};\ 0.5h \le L_i < h \\ R_{10}\left(\sum R_i \& \sum A_i \& \sum L_i\right) & s.t.: 0.75r \le R_i < 1.25r;\ 0 \le A_i < 0.33\theta_{ncc};\ 0.5h \le L_i < h \\ R_{11}\left(\sum R_i \& \sum A_i \& \sum L_i\right) & s.t.: 0.75r \le R_i < 1.25r;\ 0.33\theta_{ncc} \le A_i < 0.66\theta_{ncc};\ 0.5h \le L_i < h \\ R_{12}\left(\sum R_i \& \sum A_i \& \sum L_i\right) & s.t.: 0.75r \le R_i < 1.25r;\ 0.66\theta_{ncc} \le A_i < \theta_{ncc};\ 0.5h \le L_i < h \\ R_{13}\left(\sum R_i \& \sum A_i \& \sum L_i\right) & s.t.: 0.75r \le R_i < 1.25r;\ \theta_{ncc} \le A_i < 0.33\theta_{rcc} + \theta_{ncc};\ 0.5h \le L_i < h \\ R_{14}\left(\sum R_i \& \sum A_i \& \sum L_i\right) & s.t.: 0.75r \le R_i < 1.25r;\ 0.33\theta_{rcc} + \theta_{ncc} \le A_i < 0.66\theta_{rcc} + \theta_{ncc};\ 0.5h \le L_i < h \\ R_{15}\left(\sum R_i \& \sum A_i \& \sum L_i\right) & s.t.: 0.75r \le R_i < 1.25r;\ 0.66\theta_{rcc} + \theta_{ncc} \le A_i < \theta_{rcc} + \theta_{ncc};\ 0.5h \le L_i < h \\ R_{16}\left(\sum R_i \& \sum A_i \& \sum L_i\right) & s.t.: 0.75r \le R_i < 1.25r;\ \theta_{rcc} + \theta_{ncc} \le A_i < \theta_{rcc} + \theta_{ncc} + 0.33\theta_{lcc};\ 0.5h \le L_i < h \\ R_{17}\left(\sum R_i \& \sum A_i \& \sum L_i\right) & s.t.: 0.75r \le R_i < 1.25r;\ \theta_{rcc} + \theta_{ncc} + 0.33\theta_{lcc} \le A_i < \theta_{rcc} + \theta_{ncc} + 0.66\theta_{lcc};\ 0.5h \le L_i < h \\ R_{18}\left(\sum R_i \& \sum A_i \& \sum L_i\right) & s.t.: 0.75r \le R_i < 1.25r;\ \theta_{rcc} + \theta_{ncc} + 0.66\theta_{lcc} \le A_i < \theta_{rcc} + \theta_{ncc} + \theta_{lcc};\ 0.5h \le L_i < h \end{cases} \quad [11]$$

Where R, A and L are distance map images with values for each pixel *i* defined as the radial, angular and longitudinal distance respectively (Eq. [11]) relative to a point located at the STJ plane and centered in relation to the aortic annulus section Calcium detection (shape overlap method). The procedure finds all pixels that satisfy the cylindrical thresholding criteria in each dimension and then combines all the identified pixels via an intersection/Boolean and operation &. The flowchart of the calcification topographic mapping pipeline is shown in *Figure S1* and *Table S2*, 3D distance image views of the quantification maps on top of the valve surface and the ROI, are shown in *Figure 5A-5F*. The final conformal representation of the measured regional quantities is presented in *Figure 5G-5J*.

Normalization of the metrics

For normalizing the volume scores (Vs_d) of the contrast scores, we defined an approximation of annular radius from the annular area that was measured using CT for all patients as follows (54):

$$Indexed\ Contrast\ Calcific\ Volume = \frac{Vs}{Annular\ area} \quad [12]$$

We then estimated the annular radius of a circular aortic annulus using the area as follows:

$$Annular\ radius = \frac{\sqrt{\dfrac{Annular\ area}{\pi}}}{2} \qquad [13]$$

This normalization procedures are critical to interpret the proposed metrics in the presence of variabilities in valve dimensions, patient size and gender variability (55).

References

46. Ahrens J, Geveci B, Law C. ParaView: An End-User Tool for Large-Data Visualization. In: The Visualization Handbook. 2005.

47. Johnson HJ, McCormick MM. The ITK Software Guide Book 2: Design and Functionality, 4th edition. 552.

48. McCormick M, Liu X, Jomier J, Marion C, Ibanez L. ITK: enabling reproducible research and open science. Front Neuroinform 2014;8:13.

49. Visual Computing for Medicine. Elsevier; 2014 [cited 2021 May 13]. Available online: https://linkinghub.elsevier.com/retrieve/pii/C2011005785X

50. Johnson HJ, McCormick MM, Ibanez L. The ITK Software Guide Book 2: Design and Functionality - Volume 2. Clifton Park, NY, USA: Kitware, Inc.; 2015.

51. Schroeder W, Martin K, Lorensen B. The visualization toolkit: an object-oriented approach to 3D graphics. visualize data in 3D - medical, engineering or scientific; build your own applications with C++, Tcl, Java or Python; includes source code for VTK (supports Unix, Windows and Mac). 4th ed. Clifton Park, NY: Kitware, Inc.; 2006:512.

52. Lehmann G. Label object representation and manipulation with ITK. The Insight Journal 2007 Aug 1 [cited 2022 Mar 15]. Available online: https://www.insight-journal.org/browse/publication/176

53. Pawade T, Sheth T, Guzzetti E, Dweck MR, Clavel MA. Why and How to Measure Aortic Valve Calcification in Patients With Aortic Stenosis. JACC Cardiovasc Imaging 2019;12:1835-48.

54. Tustison NJ, Gee J. Introducing Dice, Jaccard, and Other Label Overlap Measures To ITK. The Insight Journal 2009 Dec 3 [cited 2022 Mar 16]. Available online: https://www.insight-journal.org/browse/publication/707

55. Clavel MA, Messika-Zeitoun D, Pibarot P, Aggarwal SR, Malouf J, Araoz PA, Michelena HI, Cueff C, Larose E, Capoulade R, Vahanian A, Enriquez-Sarano M. The complex nature of discordant severe calcified aortic valve disease grading: new insights from combined Doppler echocardiographic and computed tomographic study. J Am Coll Cardiol 2013;62:2329-38.